ORIGINAL PAPER

Probabilistic Response Analysis of Nonlinear Tristable Energy Harvester Under Gaussian Colored Noise

Pankaj Kumar[1] · S. Narayanan[2]

Abstract

Purpose In this paper, probabilistic response and performance analysis of a nonlinear tri-stable energy harvesting with piezoelectric coupling driven by exponentially correlated Gaussian colored noise are investigated. The effects of the system parameters, depth of potential well function, noise intensity and its correlation time on the mean square voltage are studied.
Methods The joint probability density function (PDF) as well as the voltage generated are obtained by numerically solving the four dimensional Fokker-Plank (FP) equation for the coupled electromechanical system. The results as obtained using the FP solution are verified using the Monte Carlo simulations (MCS).
Results A relative comparison of single, double and triple well potential functions on energy harvesting is presented. It is observed that the electromechanical coupling coefficient, damping ratio, intensity of noise and time constant and the shape of the potential wells have significant effects on the harvested energy. Under random excitation, for lower intensity of noise the energy harvester with single potential well outperforms the harvester with multiple deep potential wells. Beyond a threshold value of noise intensity, energy harvester with multiple well potentials outperforms as the jump from one potential well to another becomes more frequent with inter-well dynamics functioning. It is found that the probability of jumps between potential wells is enhanced with increase in the noise intensity and corresponding increase in the mean power generation. Nevertheless, this enhancement is weakened with increase in correlation time of noise.
Conclusion The study has shown that, the energy harvested can be optimized by suitable choice of the potential function, coupling parameters, the noise intensity and its correlation time.

Keywords Piezoelectric energy harvesting · Multi-well potentials · Fokker-Planck equation · Optimal energy harvesting parameters

Introduction

Vibrational energy harvesting (VEH) is a clean and sustainable energy source and has become popular recently due to its potential to generate continuous energy from harvesting widely available environmental vibrations in real-life application such as wind flow [1], human activities [2], ocean waves [3], machine operation [4]. It finds applications to power low-energy devices such as charging batteries of electronic devices, wireless sensors, implantable electronics for safety monitoring devices, biomedical engineering and microelectro-mechanical system applications [5–9]. The linear vibratory energy harvester, represented as a linear spring–mass–damper system coupled with piezoelectric [5, 10, 11] or electromagnetic [12] or electrostatic [13] transduction mechanism, operates based on the principle of resonance limiting its effectiveness only to a very narrow effective frequency bandwidth close to the resonance frequency [5]. Moreover, natural frequencies for miniaturized VEH are in order of kilohertz [14], while environmental excitations have frequency in the range of $0 - 30$Hz. To make VEH more effective over a broader frequency range, random excitations and various techniques of nonlinearities such as bistability [10, 15, 16], multistabilty [17–20], plucking frequency-up conversion [21], passive or active frequency tuning [22] have been introduced in the design of VEH [6–8, 11]. Due to the unique advantages

✉ Pankaj Kumar
pankajiit1@yahoo.co.in

S. Narayanan
narayans@iitm.ac.in

[1] Vibration Analysis Group, Bharat Heavy Electricals Limited, Nagpur 440001, India

[2] Mechanical Engineering, Indian Institute of Technology Madras, Chennai 600036, India

Springer

of stiffness nonlinearity, the nonlinear based VEH model has a wider frequency bandwidth resulting in enhanced broadband performance of VEH. The analysis of nonlinear vibration energy harvester subjected to random excitations thus has been investigated widely in the literature [7, 8, 15, 19].

Nonlinear oscillators with different potential energy functions, such as monostable [23], bistable [7, 8] and tristable [19] potential wells have been received considerable attention recently in the design of VEH systems. Several design models such as a cantilever beam with magnetic repulsion [17, 18], ferromagnetic beam with magnetic attraction [17, 18], magnetic levitation [24], buckling beam [25] and buckling plate [26] have been proposed in the context of bistable VEH. Compared to the linear model, they are found to enhance the effectiveness of the vibration energy harvesters (VEH) over a wider frequency range due to activation of large inter-well escape mechanism.

Sebald[27] investigated the Duffing oscillator with piezoelectric electromechanical coupling and excited with sine bursts or colored noise as VEH and showed that big gain in bandwidth performance is possible when the VEH is nonlinear. They also observed that monostable VEH behaves very similar to a linear model. Daqaq [23] theoretically investigated a nonlinear monostable VEH and observed that it does not outperform the linear counterpart under broadband random excitation. To overcome these difficulties, the concept of multi-modal VEH is proposed. A significant number of theoretical and experimental investigations on bistable energy harvester under Gaussian white noise excitation [7, 8, 10, 16, 28] showed direct correlation between the power output and the noise intensity. He and Daqaq [28] used statistical linearization techniques to investigate the effect of potential function asymmetries on the performance of nonlinear VEHs under Gaussian white noise excitations and found that VEH with a symmetric bistable potential produced higher output power. Narayanan et al.[16] derived closed-form approximate solution for the mean harvested power and derived the optimal design parameters under broadband random ambient excitations such that the harvested power is maximized. Adhikari et al. [10] using the theory of random vibrations investigated a piezoelectric based VEH subjected to random base excitation and derived exact closed-form expressions for mean output power. Jiang and Chen [29] using the stochastic averaging method derived the exact stationary solution of the averaged Fokker Planck (FP) equation and observed that quadratic nonlinearity alone or combined with appropriate cubic nonlinearities can improve the performance of a nonlinear VEH under Gaussian white noise excitation. Kumar et al.[8] numerically solved the three dimensional FP equation associated with bistable VEH and obtained the optimal system parameter under ambient Gaussian white noise excitation for maximum power output. They observed a threshold value of the noise intensity for activation of desirable inter-well motion in a bistable VEH.

Recently, new class of energy harvesters with triple potential wells has been proposed to improve the broadband performance

of randomly excited VEH [19]. Several design philosophies such as cantilever beam with a tip magnet [17], ferromagnetic beam [17], spring based configuration [30], magnetic levitation [31] are used in this context. Due to the shallower potential barrier, longer distance between outermost stable equilibrium points, lower potential barrier and having better stable state than the bistable VEH, tristable VEH has advantages over the bistable VEH [17]. The influence of potential well depth for a tristable energy harvesting under deterministic excitation was experimentally investigated in [19]. They found that the tristable VEH with shallower potential enhanced the broadband performance and also has smaller threshold of input energy for inter potential well motion. For stochastic excitation also relatively lower noise intensity is required to trigger the inter-well motion.

Most of the investigation of VEH systems has considered either deterministic or Gaussian white noise excitations [7, 8, 10, 16, 19, 28]. White noise with delta function correlation time is a idealized model to represent broad band excitation. However, in practice, random excitations have a finite correlation time, though small [10, 32] and hence the effect of temporal correlation has to be taken into consideration. For this reason the Gaussian colored noise (Ornstein-Uhlenbeck process) having non-zero correlation time has been attracting attention as a realistic model to approximate the ambient vibration [33, 34]. In the context of the energy harvesting problem, a piezomagnetoelastic VEH under exponentially correlated Gaussian colored noise, increases the state-space dimension of the problem involving the solution of a corresponding four-dimensional Fokker–Planck–Kolmogorov(FPK) equation, adding numerical difficulties in the solution procedure. Hence, approximate methods have been used to numerically investigate the performance of VEH under colored noise excitation. Using the stochastic averaging method, Liu et al. [35] investigated the probabilistic response of nonlinear VEH driven by exponentially correlated Gaussian colored noise. Zhang et al. [20] investigated the stochastic bifurcations and the performance of an inductive type power generator with a tristable potential function driven by colored Gaussian noise. They employed stochastic averaging method to derive the averaged FPK equation and obtained the PDF of the amplitude. Using the stochastic averaging method, Xiao et al. [11] investigated monostable duffing-type VEH with piezoelectric coupling under correlated multiplicative and additive white noise and observed that the mean output power first increases with increasing ratio of the time constant reaches a maximum and then decreases.

In this paper, the effectiveness of single, double- and triple-well potential wells on energy harvesting under exponentially correlated Gaussian colored noise is investigated. In the case of random excitation, the finite difference(FD) method is used to solve the corresponding Fokker-Planck (FP) equation giving the joint probability density functions (JPDF) of the response and the voltage generated. The electromechanical coupling coefficient, damping ratio, intensity of noise and time constant and

the shape of the potential wells have significant effects on the harvested energy. For very low noise levels, the energy harvester with single potential well outperforms the harvester with multiple deep potential wells. Energy harvesters with multiple well potentials perform better with higher noise levels as the response increases and jumps from one potential well to another with inter-well dynamics operating. Hence the depth and distributed positions of potential wells are factors which directly influence the performance of multistable VEH. It is found that the probability of jumps between potential wells are enhanced with increase in the noise intensity and corresponding increase in the mean power generation. However, this enhancement is weakened with increase in correlation time of excitation. The mean output power first increases with increase in the quintic stiffness, reaches a maximum and then decreases. The conflicting interplay of the oscillator parameters including the shape of the potential wells leads to an optimization problem for maximum energy harvesting, which is also considered in this paper. The estimated PDFs as obtained using the FP solution are verified using Monte Carlo simulation (MCS) studies.

Mathematical Model of Multistable Energy Harvester

VEH with multi-potential wells can be constructed by coupling the nonlinear oscillator to an electrical circuit as shown in Fig. 1(a). The ferromagnetic cantilever beam [6] is supported between two symmetric permanent magnets with the variable inclination angles, near the free end and subjected to support random excitation. The tip of the cantilever too has a magnet which acts as proof mass and its interaction with the other two magnets produce a magnetic force. In addition to the monostable state, the multi stable configuration such as bistable and tristable states can be obtained by

adjusting the design parameters of magneto-elastic interaction. Piezoelectric layers are bonded to the cantilever beam near the root and connected to an electrical load. The voltage generated from the piezoelectric layers across the load due to the random excitation contributes to the energy harvesting.

The coupled nonlinear electromechanical equations of the motion of tristable VEH, governing the system first natural mode and electric voltage generated can be written in the following form [7]

$$m\ddot{X} + c\dot{X} + \bar{U}'(X) - \theta V = -m\ddot{X}_b, \tag{1}$$

$$C_p \dot{V} + \frac{V}{R_l} + \theta \dot{X} = 0, \tag{2}$$

where X represents the relative transverse displacement of the beam tip with respect to support motion X_b, V is the voltage output across the load resistance R_l, c is a linear viscous damping coefficient, θ is a linear piezoelectric coupling coefficient in the two equations, C_p is the capacitance of the piezoelectric material, $\ddot{X}_b$ is the stochastic support acceleration, $\bar{U}'(X)$ is the potential energy function of the mechanical system which depends on the nonlinearity present in the harvester, ($'$) denotes differentiation with respect to X and the dot represents the derivative with respect to time t. In this work, potential energy function is chosen in the following general form

$$\bar{U}(X) = \frac{1}{2}\bar{k}_1 X^2 + \frac{1}{4}\bar{k}_3 X^4 + \frac{1}{6}\bar{k}_5 X^6, \tag{3}$$

where $\bar{k}_1$, $\bar{k}_3$ and $\bar{k}_5$ are respectively the linear, cubic and quintuple nonlinear stiffness coefficients.

With the appropriate change of variables, Eqs. (1) and (2) can be rewritten in the following form as

$$\ddot{X} + 2\zeta\omega_n\dot{X} + \frac{\mathrm{d}U(X)}{\mathrm{d}X} - \chi V = \xi(t), \tag{4}$$
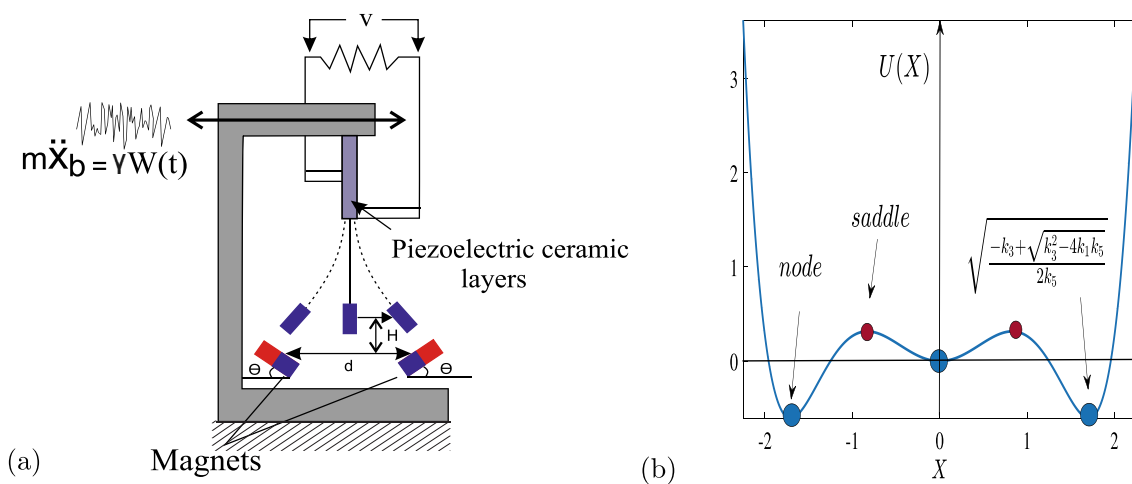

Fig. 1 **a** Schematic of a tristable piezomagnetoelastic cantilever beam subjected to random base excitation, **b** tristable potential function

$$\dot{V} + \lambda V + \beta \dot{X} = 0, \tag{5}$$

where $\zeta = c/2m\omega_n$, $U(X) = \frac{1}{2}k_1X^2 + \frac{1}{4}k_3X^4 + \frac{1}{6}k_5X^6$, $k_1 = \bar{k}_1/m$, $k_3 = \bar{k}_3/m$, $k_5 = \bar{k}_5/m$, $\ddot{X}_b = \xi(t)$, $\lambda = 1/R_lC_p$, $\beta = \theta/C_p$, $\chi = \theta^2/k_1C_p$.

Regardless of the coupling mechanism, chosen potential energy function permits Eqs. (4) and (5) to characterize the different kind of dynamics for the nonlinear energy harvesting system. When $k_3^2 - 4k_1k_5 < 0$ nonlinear energy harvesting system will have only one fixed point at the origin and hence $U(X)$ will have monostable potential. For $k_1 > 0$, $k_3 < 0$, $k_5 > 0$ and $k_3^2 - 4k_1k_5 > 0$, system has five fixed points at $(0,0), (\sum_{j=1}^{4} X_j, 0)$, where $X_{1,2} = \pm\sqrt{\gamma_1}$, $X_{3,4} = \pm\sqrt{\gamma_2}$, $\gamma_{1,2} = \frac{-k_3 \pm \sqrt{k_3^2 - 4k_1k_5}}{2k_5}$. Out of these five fixed points $(0,0)$, $(X_1, 0)$ and $(X_2, 0)$ are stable equilibrium nodes, while $(X_3, 0)$ and $(X_4, 0)$ are saddle nodes and $U(X)$ will have tristable potential function as shown in Fig. 1(b). Moreover, as shown in Figs. 2(a) and (b) both depth and span of two symmetric wells depend on the stiffness parameter k_3 and k_5. With the decrease of either k_3 or k_5, the potential well barrier increases and, hence, inter-well motion between two consecutive wells will be restricted.

We assume ambient random excitation $\xi(t)$ in Eq. (4) as Gaussian colored noise (Ornstein-Uhlenbeck process) with zero mean and an exponentially decaying correlation function as follows (Fig. 3(a))

$$\begin{aligned} E[\xi(t)\xi(s)] &= \frac{D}{\tau} \exp\left[-\frac{|t-s|}{\tau}\right] \\ &= \frac{\sigma^2}{2\tau} \exp\left[-\frac{|t-s|}{\tau}\right], \end{aligned} \tag{6}$$

where $\sigma = \sqrt{2D}$ measures the intensity of Gaussian colored noise, the characteristic time τ denotes the correlation time of the noise. The power spectral density of $\xi(t)$ can be expressed as (Fig. 3(b))

$$S_\xi(\omega) = \frac{2D}{1 + \tau^2\omega^2}. \tag{7}$$

An idealized condition when $\tau \to 0$, the colored noise $\xi(t)$ tends to the white noise process $W(t)$ which has the following statistical properties

$$E[W(t)] = 0, \quad E[W(t)W(s)] = \sigma^2\delta(t-s), \quad \sigma^2 = 2D, \tag{8}$$

where D is the spectral density of the white noise and $\delta(\cdot)$ is the Dirac-delta function.

The time evolution of such exponentially correlated Gaussian colored noise $\xi(t)$ can be conveniently expressed in terms of the white noise $W(t)$ in the following form

$$\dot{\xi}(t) = -\frac{1}{\tau}\xi + \frac{1}{\tau}W(t), \tag{9}$$

where $W(t) = \sigma dB(t)/dt$, is the mean zero stationary Gaussian white noise process and $B(t)$ is the unit Wiener process.

Fokker–Planck Equation of VEH

Introducing the variables $X_1 = X$, $X_2 = \dot{X}$, $X_3 = V$ and $X_4 = \xi$, Eqs. (4), (5) and (9) can be expressed in terms of a set of first order Itô type stochastic differential equation (SDE) of the form
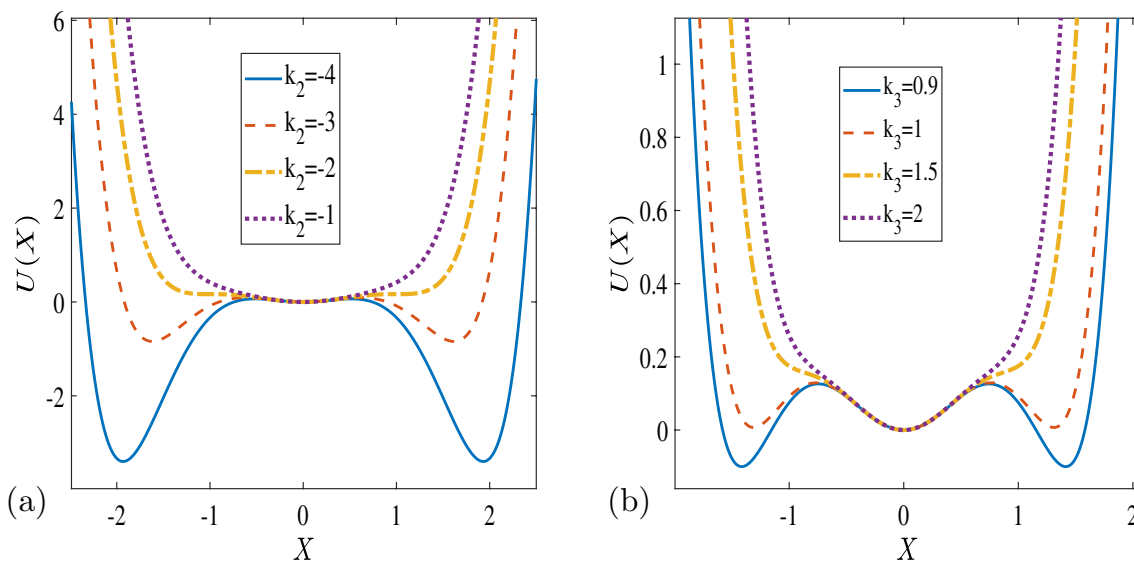

Fig. 2 Potential energy for (**a**) $k_1 = 1, k_5 = 1$ and different values of k_3; (**b**) $k_1 = 1, k_3 = -2.3$ and different values of k_5
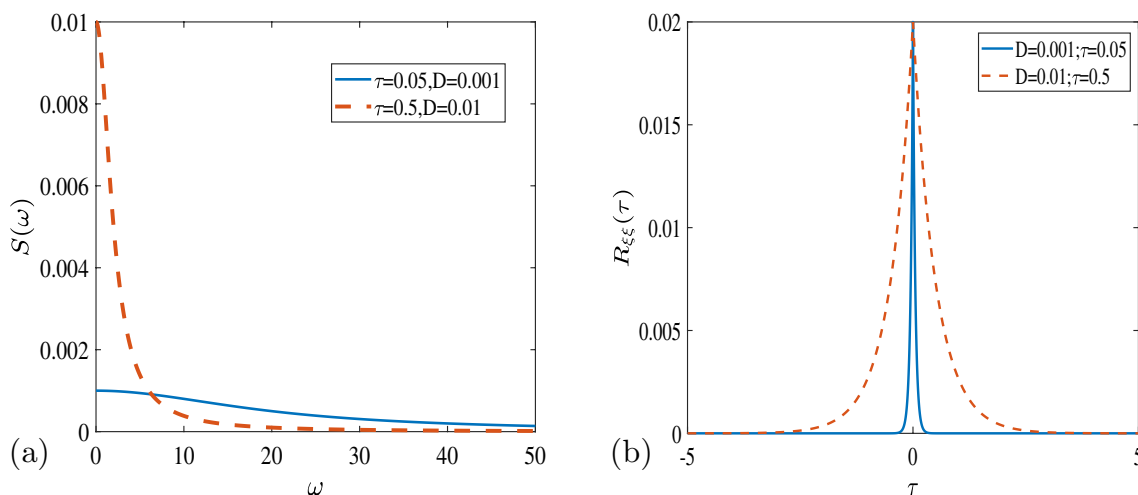
Fig. 3 **a** Auto-correlation and **b** spectral densities for the Gaussian colored noise

$$\begin{Bmatrix} dX_1(t) \\ dX_2(t) \\ dX_3(t) \\ dX_4(t) \end{Bmatrix} = \begin{bmatrix} X_2 \\ -k_1X_1 - k_3X_1^3 - k_5X_1^5 - 2\zeta\omega_nX_2 + \chi X_3 + X_4 \\ -\beta X_2 - \lambda X_3 \\ -\frac{1}{\tau}X_4 \end{bmatrix}$$

$$dt + \begin{Bmatrix} 0 \\ 0 \\ 0 \\ \frac{\sqrt{2D}}{\tau} \end{Bmatrix} dB(t),$$

(10)

where $dB(t) = B(t_{n+1}) - B(t_n) \sim \sqrt{t_{n+1} - t_n}N(0,1)$ is the unit Wiener process increment and $N(0, 1)$ is the unit normal random variate. For Gaussian white noise excitation, the response state vector $\mathbf{X} = [X_1, X_2, X_3, X_4]^T$ corresponding to Eq. (10) of the energy harvesting system is Markovian and consequently the time evolution of the joint PDF p will be governed by the following four-dimensional FP equation [36]

$$\begin{aligned} \frac{\partial p}{\partial t} = &-X_2\frac{\partial p}{\partial X_1} + (2\zeta\omega_nX_2 + k_1X_1 \\ &+ k_3X_1^3 + k_5X_1^5 - \chi X_3 - X_4)\frac{\partial p}{\partial X_2} + \\ &(\beta X_2 + \lambda X_3)\frac{\partial p}{\partial X_3} + \frac{1}{\tau}\frac{\partial p}{\partial X_4} \\ &+ \frac{\sigma^2}{2\tau^2}\frac{\partial^2 p}{\partial X_4^2} + (2\zeta\omega_n + \lambda)p, \end{aligned}$$

(11)

where p is the joint PDF of the state variables $\mathbf{X}$. The stationary joint probability density function (PDF) of the response variables of the corresponding four-dimensional FP equation ($\frac{\partial p}{\partial t} = 0$) of VEH is numerically obtained using the FD method [37, 38]. The response statistics, the mean square voltage and the mean square displacement of the

VEH are obtained from the respective joint PDFs. The time histories for the state variables associated with VEH are obtained by direct numerical integration of Eq. (10) using the Euler–Maruyama method [39].

To compare the accuracy of the FP solution, the estimated PDF for the state variables as obtained using the FD method is compared with those obtained from Monte Carlo simulation (MCS) scheme. The MCS is a direct numerical integration technique [40, 41], which involved the numerical simulation for the increments of a Wiener process $dB(t)$ and numerical integration of the SDEs as in Eq. (10) to each discrete excitation using the forward Euler–Maruyama (EM) integration scheme [39, 40]. In this work, to estimate the stationary PDF for the state variables using MCS, on the average, 2×10^5 realizations with a time step $dt = 0.0005$ have been used to integrate the governing set of four coupled first order SDE as in Eq. (10) using the forward EM numerical integration until the steady state is achieved.

Numerical Results

The dynamics of the piezomagnetoelastic nonlinear energy harvester represented by Eqs. (4), (5) and (9) is numerically investigated. The following system parameters $\omega_n^2 = 1$, $k_1 = 1$, $\lambda = 0.05$, $\beta = 0.5$ and $\chi = 0.05$ for the oscillator are kept fixed in most of the investigations. The coefficients of the nonlinear terms k_3 and k_5, electromechanical coupling parameter λ, piezoelectric coupling coefficient χ, the damping ratio ζ, noise intensity σ and its correlation time τ are varied.

To better understand the effect of noise intensity and its correlation time of the colored noise on the performance

of the tristable VEH, the variations of mean square electric voltage with respect to noise intensity σ and correlation time τ are shown in Fig. 4(a). The other parameters adopted for the oscillator are $\zeta = 0.05$, $k_3 = -2.3$ and $k_5 = 1$. It can be seen from Fig. 4(b) that for a given correlation time τ of Gaussian colored noise, the mean square voltage almost increases proportionally with the excitation intensity. However, for a given noise intensity, increase of the correlation time reduces the mean output power. Hence the increase of correlation time of the colored noise will weaken the performance of the VEH. Figure 4(b) presents the mean square voltage for the case of Gaussian white noise excitation ($\tau \to 0$). It can be seen that for the given noise intensity, E[V^2] increases with decrease in correlation time τ; however, this increase is not perceptible for lower values of correlation time. For the given system parameters, the mean square electric voltage for the colored noise having correlation time $\tau = 0.025$ is almost the same for white noise.

Figure 5 shows the JPDF of X_1 and X_2 for four values of σ and for $\zeta = 0.025$, $\tau = 1$. For low intensity of excitation $\sigma = 0.05$ the joint PDF is unimodal at origin. For the noise intensity to $\sigma = 0.08$, the peak value at origin decreases and almost vanishes and two symmetric peaks appear in the joint PDF. For further increase in the noise intensity, the peak at the origin starts to gain strength and subsequently at $\sigma = 0.25$, the VEH has a tri-modal joint PDF. This signifies

that with increase in the noise intensity there is larger probability of the system response to move between the potential wells and hence the increase in the mean power output. The marginal PDF of the voltage as obtained using the FP and MCS solutions corresponding to Fig. 5 is shown in Fig. 6, having the excellent agreement of the FP solution with the MCS results and hence validating the numerical solution of the FP equation.

Next for a given noise intensity $\sigma = 0.1$, Fig. 7 shows the JPDF of X_1 and X_2 for four values of noise correlation time τ, which clearly indicates that increasing the correlation time has the opposite effect to that of noise intensity. For increased τ, the center peak intensity reduces, transforming to tri-modal and then to bimodal and finally to unimodal behavior. The marginal PDF of the voltage as obtained using the FP and MCS solutions corresponding to Fig. 7 is shown in Fig. 8, once again showing the good agreement between the two.

Figures 9 and 10 present the impact of viscous damping ratio ζ on the mean square voltage for different correlation time of Gaussian colored noise and its intensity. The other parameters adopted for the oscillator are $k_3 = -2.3$ and $k_5 = 1$. For a given value of the noise intensity as the damping ratio ζ increases the mean square voltage significantly reduces. Figure 9(b) presents the mean square voltage for the case of Gaussian white noise excitation. As mentioned earlier the mean square electric voltage for the Gaussian white noise excitation is almost the same as for the case of colored noise having correlation time $\tau = 0.025$. Figure 11 shows the JPDF of X_1 and X_2 for three values of ζ and for $\sigma = 0.1$, $\tau = 0.025$. The three separate peaks in the JPDF tend to come closer as ζ decreases and merges for $\zeta = 0.0125$. This signifies that there is larger probability of the system response to move between the potential wells for lower values of ζ. For higher damping, there is higher probability of the response staying in the neighborhood of the stable equilibrium points of the deterministic system and the probability of the response to move between potential wells is negligible.

Figures 12 and 13 present the effects of the quintic stiffness coefficient k_5 on the mean square voltage for different correlation time of Gaussian colored noise and damping coefficient respectively. The other parameters adopted for the oscillator are $k_3 = -2.3$ and $\sigma = 0.1$. As shown in Fig. 12(b), for the given oscillator parameters as the correlation time reduces, mean square electric voltage increases and is maximum for the Gaussian white noise. Figure 13 shows the variation of mean square voltage as a function of the nonlinear stiffness parameter k_5 for three damping coefficients $\zeta = 0.0125, 0.025$ and 0.05. For a given value of the correlation time or the damping coefficient as k_5 increases the mean square voltage initially increases, reaches a maximum for a particular k_5 and decreases with further increase
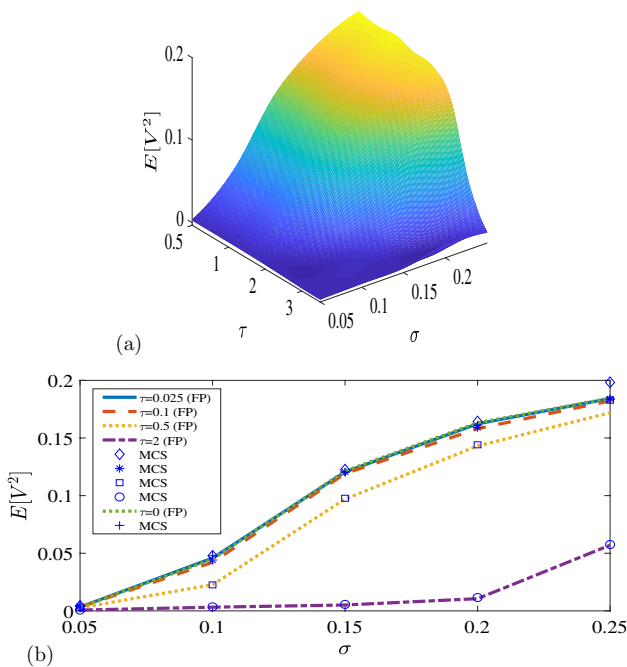

(a)

(b)

Fig. 4 **a** Mesh surface of the mean square electric voltage E[V^2] in $\sigma - \tau$ plane (**b**) variation of $E[V^2]$ with respect to noise intensity σ for different values of τ
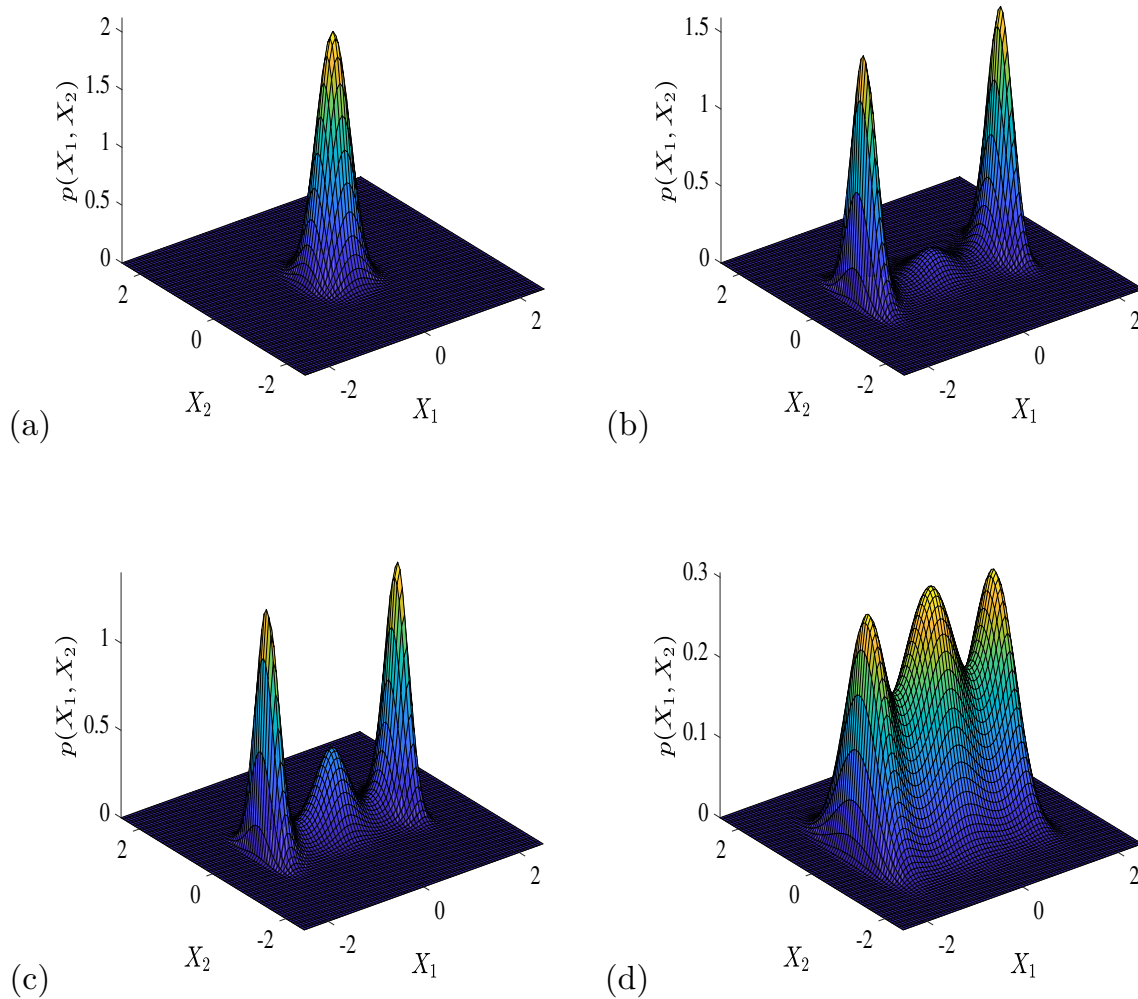
(a)

(b)

(c)

(d)

Fig. 5 Joint PDF for $k_3 = -2.3$, $k_5 = 1$, $\zeta = 0.025$, $\tau = 1$ and (**a**) $\sigma = 0.05$, (**b**) $\sigma = 0.08$, (**c**) $\sigma = 0.125$, (**d**) $\sigma = 0.25$
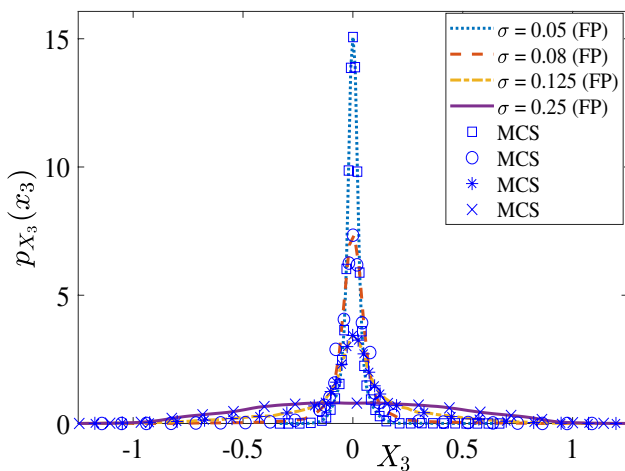

Fig. 6 Marginal PDF of voltage corresponding to Fig. 5

in k_5. Thus, it may be concluded that for a given value of the damping ratio ζ and excitation parameters, there is an optimum value of k_5 for which the mean square voltage is a maximum. As seen from Fig. 14 for the given damping coefficient, at lower value of k_5 the separation distance between the potential wells and depth of the potential wells increase and larger intensity of noise is required to enable the inter-well motion. As k_5 increases the three peaks in the JPDF merge. This signifies that there is larger probability of the system response moving from one potential well to the other. This also signifies that there is increase in the power output. With further increase in k_5 the JPDF tends to become uni-modal with the JPDF peaking around the zero equilibrium point with consequent decrease in the mean square voltage. This is the reason for the mean square voltage to attain a maximum value for a particular value of k_5.
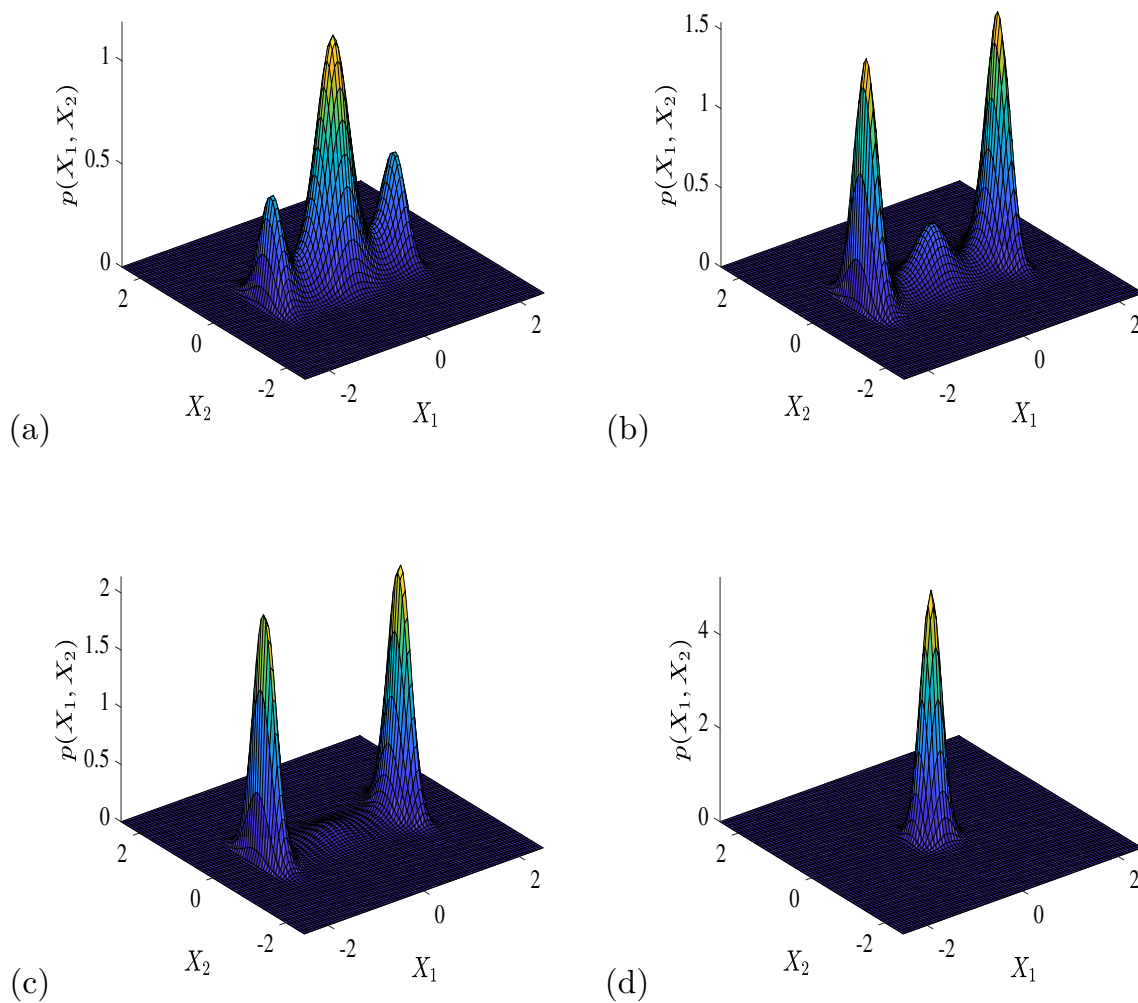
Fig. 7 Joint PDF for $k_3 = -2.3$, $k_5 = 1$, $\zeta = 0.05$, $\sigma = 0.1$ and **a** $\tau = 0.025$, **b** $\tau = 0.8$, **c** $\tau = 1$, **d** $\tau = 2$
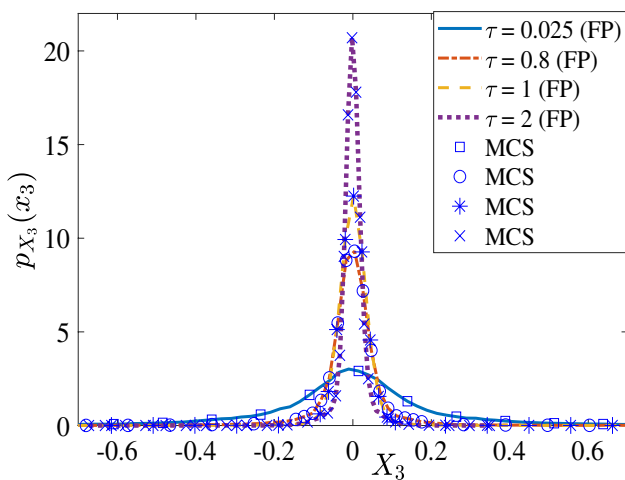

Fig. 8 Marginal PDF of voltage corresponding to Fig. 7

Figure 15 demonstrates the effect of the system parameters λ, the electromechanical coupling coefficient in the mechanical system χ and the coupling coefficient in the electrical equation β, on the mean square voltage for three different values of the damping ratio ζ for the tristable oscillator. The other parameters adopted for the oscillator are $k_3 = -2.3$, $k_5 = 1$, $\sigma = 0.1$ and $\tau = 0.0025$. The mean square voltage decreases with increase in λ, decreases slightly with increase in χ, but increases considerably with increase in β. Hence the energy harvesting capability of the nonlinear oscillator can be enhanced by proper tuning of the parameters of the system in addition with an optimum choice of the noise intensity.

Figure 16 presents a comparison of the mean square voltage for different types of potential wells as a function

Fig. 9 a Mesh surface of the mean square electric voltage $E[V^2]$ in $\zeta - \tau$ plane (**b**) variation of $E[V^2]$ with respect to damping coefficient ζ for different values of τ
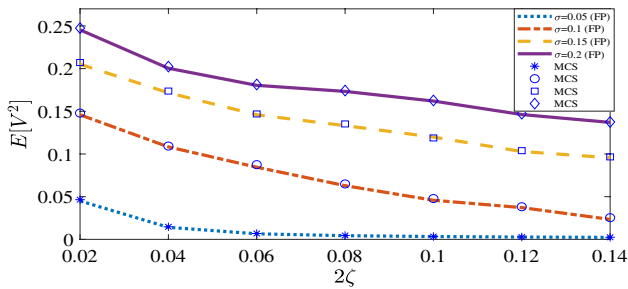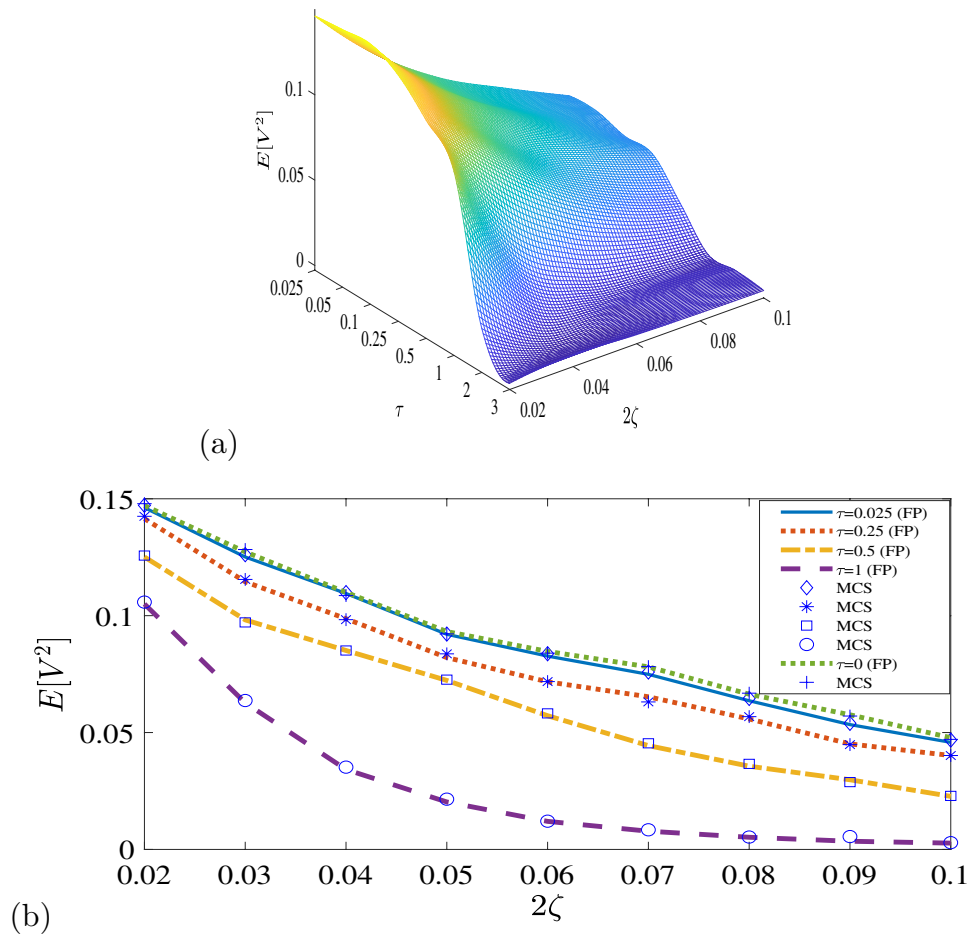

(a)

(b)

Fig. 10 Variation of the mean square electric voltage $E[V^2]$ with damping coefficient ζ for different value of noise intensity σ

of noise intensity. Four different categories of potential functions (i) linear $(k_1 > 0, k_3 = k_5 = 0)$,(ii) nonlinear monostable $(k_1 \geq 0, k_3 \neq 0, k_5 = 0)$,(iii) nonlinear bistable $(k_1 < 0, k_3 > 0, k_5 = 0)$ and (iv) nonlinear tristable

$(k_1 > 0, k_3 < -2\sqrt{k_5}, k_5 > 0)$ are chosen for comparison. Upto some threshold value of σ, the mean square voltage is very low, but it increases steeply with σ beyond this value. This behavior is irrespective of the shape of the potential wells. It is observed that the mean square voltage and hence the harvested energy is significantly larger with bistable shallow potential well and tristable potential well than with linear, monostable potential well and bistable deep potential well. Moreover, for low excitation intensity as shown in Fig. 16(b), the linear VEH performs better than the nonlinear oscillators with monostable potential well and bistable deep potential well. Time waveforms of displacement and voltage for nonlinear monostable, bistable with shallow potential and tristable VEH at $\sigma = 0.1$ corresponding to Fig. 16 are shown in Figs. 17 and 18, respectively. It can be seen that for the given noise intensity both bistable and tristable

Fig. 11 Joint PDF for
$k_3 = -2.3$, $k_5 = 1$, $\sigma = 0.1$, $\tau = 0.025$
and (**a**) $\zeta = 0.0125$, (**b**)
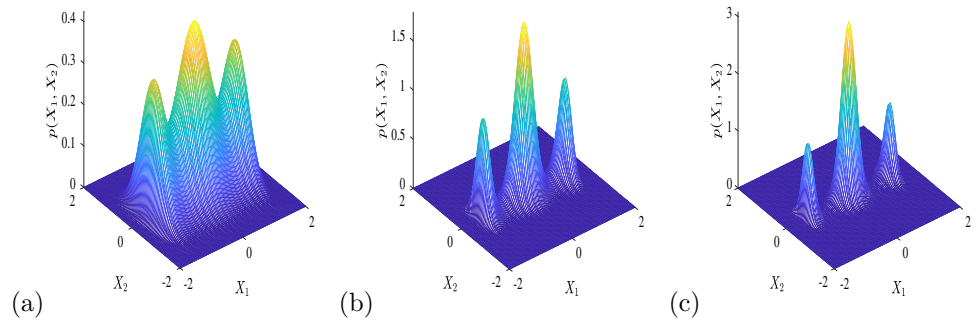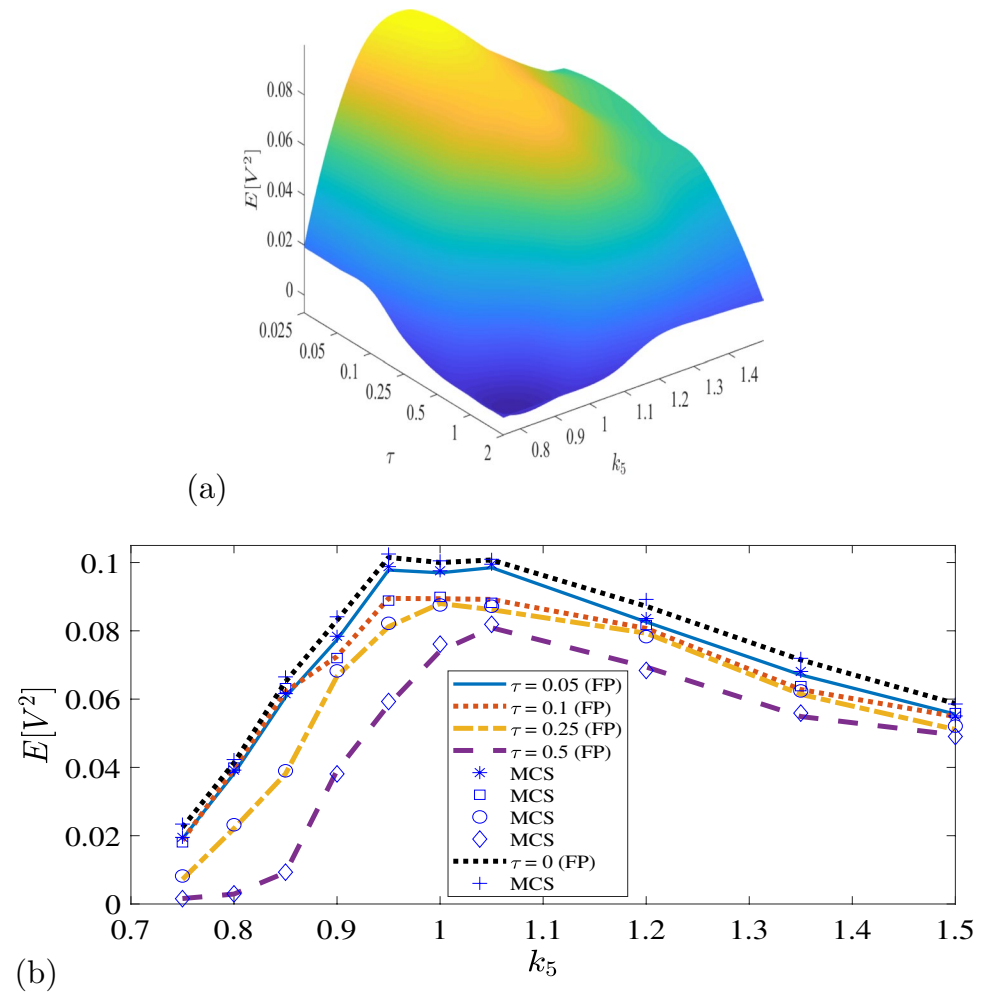$\zeta = 0.05$, (**c**) $\zeta = 0.075$

(a) (b) (c)

Fig. 12 **a** Mesh surface of the
mean square electric voltage
$E[V^2]$ in $k_5 - \tau$ plane (**b**) variation of $E[V^2]$ with respect to
nonlinear term k_5 for different
values of τ

(a)

(b)

VEH undergo frequent jumps between potential wells and produce large amplitude of response, thus generating a high output voltage, whereas for nonlinear monostable VEH, the response is restricted to a single well and the output voltage is relatively low. The mean square voltage obtained by Monte Carlo simulation (MCS) is also shown alongside which shows very good agreement with the result of the numerical solution of the FP equation solutions.
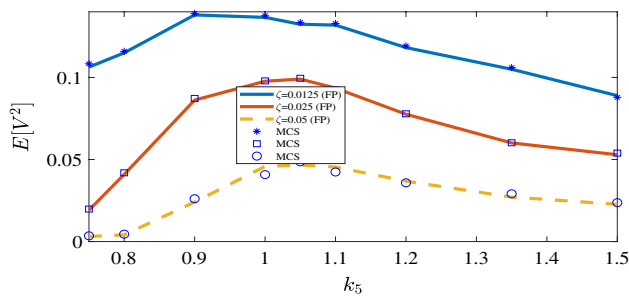
Fig. 13 Variation of the mean square electric voltage $E[V^2]$ with k_5 for different value of damping ratio ζ

Conclusions

The relative performance of piezomagnetoelastic nonlinear energy harvester with different types of potential wells under exponentially correlated Gaussian colored noise is investigated by numerical solution of the corresponding FP equation. The influence of various types of potential well functions, coupling parameters, damping coefficient and the intensity of Gaussian colored noise on the mean square voltage is investigated. The mean output power increases with an increase in the noise intensity while it decreases

with increase in the correlation time of the Gaussian colored noise which is directly linked with the stochastic transitions between the potential wells. The linear VEH outperforms a nonlinear VEH with monostable potential well and bistable deep potential well especially for low noise intensities. This may be attributed to the low probability of inter-well movement with low intensity of noise. The nonlinear VEH with bistable shallow potential well and tristable potential well outperforms the linear VEH and the nonlinear VEH with monostable potential well and bistable deep potential well significantly. In all the cases, the mean square voltage increases slowly with increase in noise intensity initially but rapidly after a threshold value of noise intensity. The higher mean square voltage of nonlinear VEH with bistable shallow potential well and tristable potential well is due to the higher probabilities of inter-well motions. The mean square voltage also varies with respect to other system parameters such as the damping coefficient c, electromagnetic coupling coefficient β and χ and the load resistance capacitance parameter λ in a complex and conflicting way which leads to an optimization problem for maximum energy harvested in terms of mean square voltage with respect to the parameters as well as the noise intensity and shape of potential wells which can be investigated further.
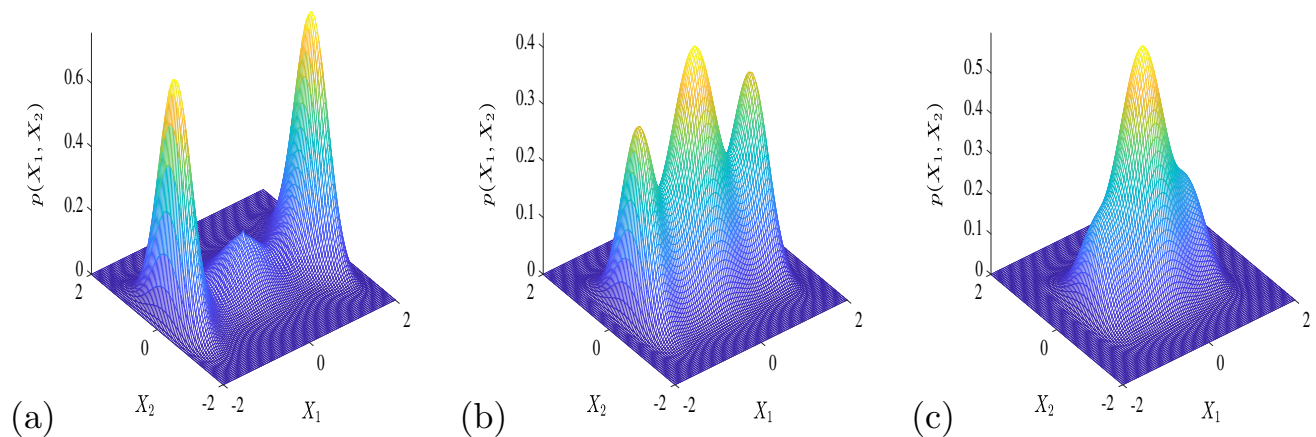

Fig. 14 Joint PDF for $k_3 = -2.3$, $c = 0.025$, $\sigma = 0.1$, $\tau = 0.025$ and (**a**) $k_5 = 0.75$, **b** $k_5 = 1$, (c) $k_5 = 1.4$
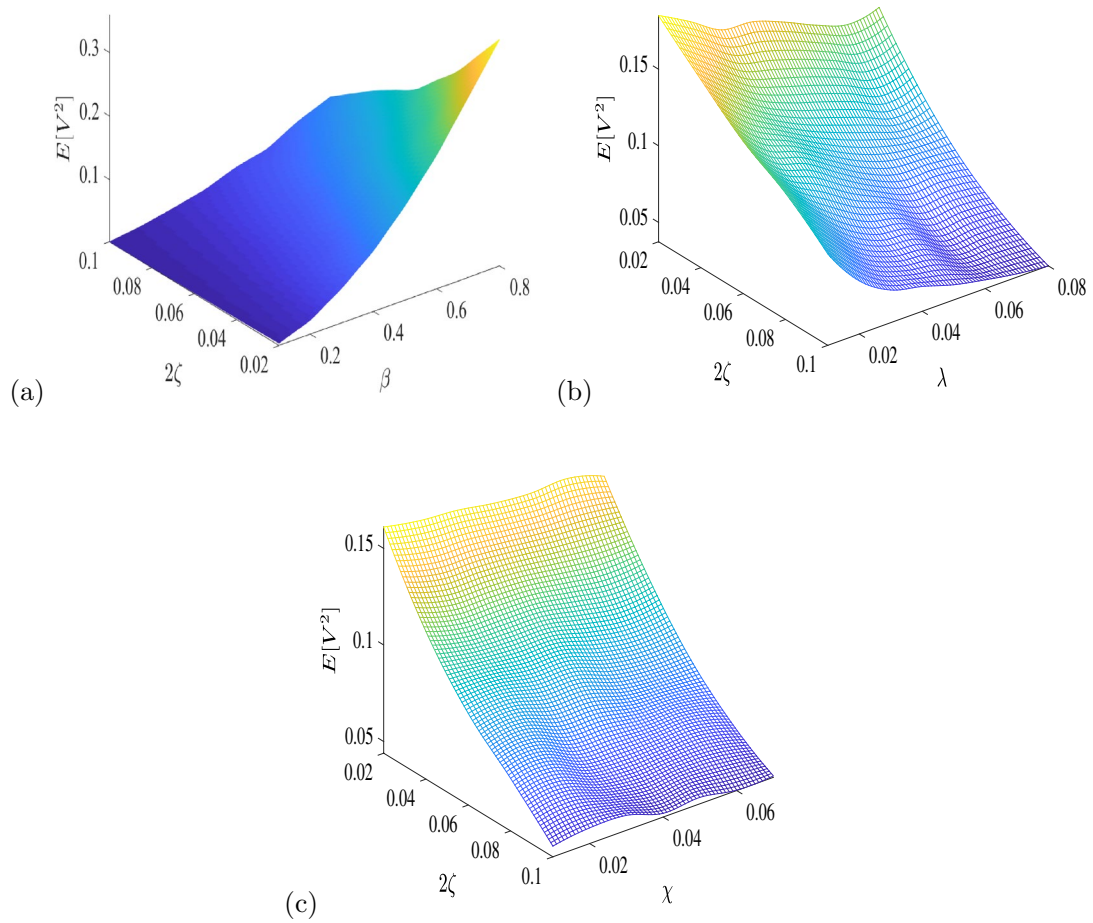
Fig. 15 Mesh surface of the mean square electric voltage E[V^2] in (**a**) $\beta - \zeta$, **b** $\lambda - \zeta$, **c** $\chi - \zeta$ plane
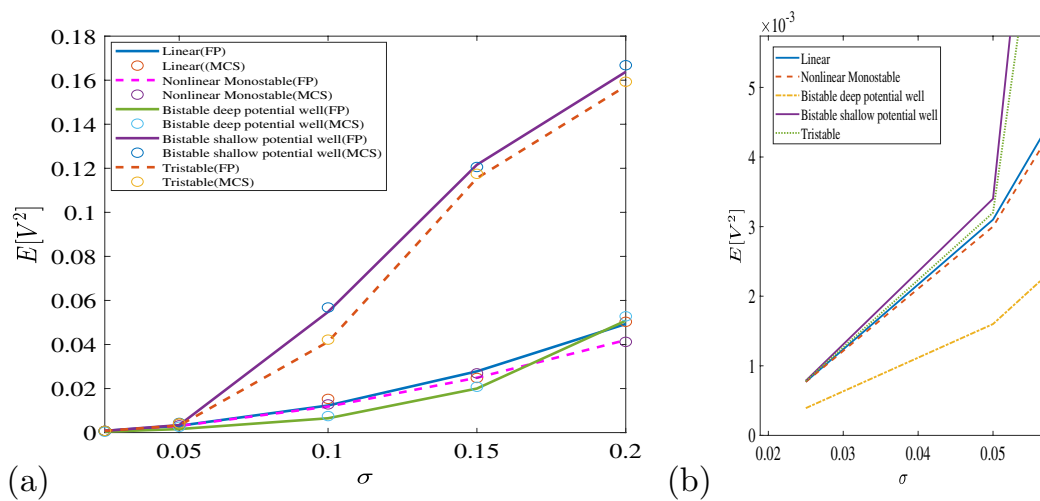

Fig. 16 A relative comparison of the mean square electric voltage E[V^2] (**a**) for different type of potential function (**b**) magnified view for low intensity; FP solution (——); MCS (∘)
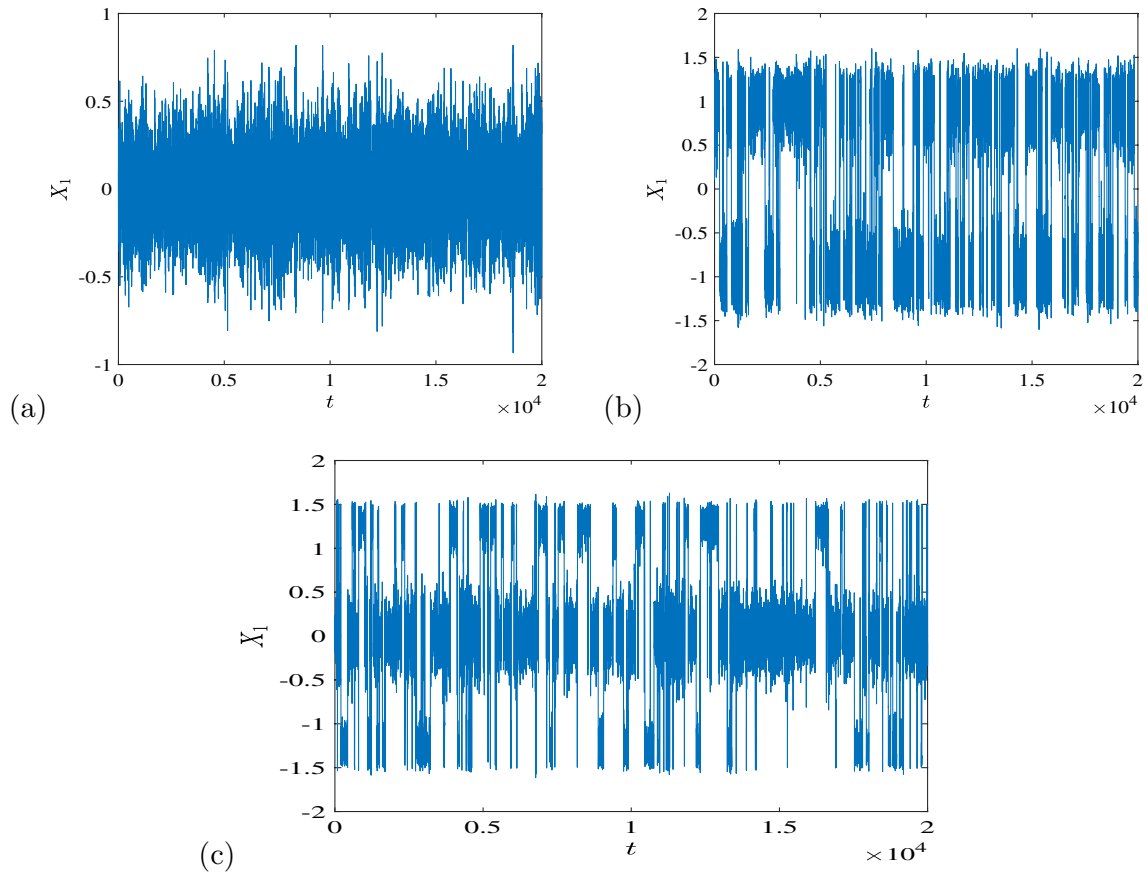
Fig. 17 Time waveform of displacement at $\sigma = 0.1$ for Fig. 16 for (**a**) nonlinear monostable, (**b**) bistable with shallow potential, (**c**) tristable
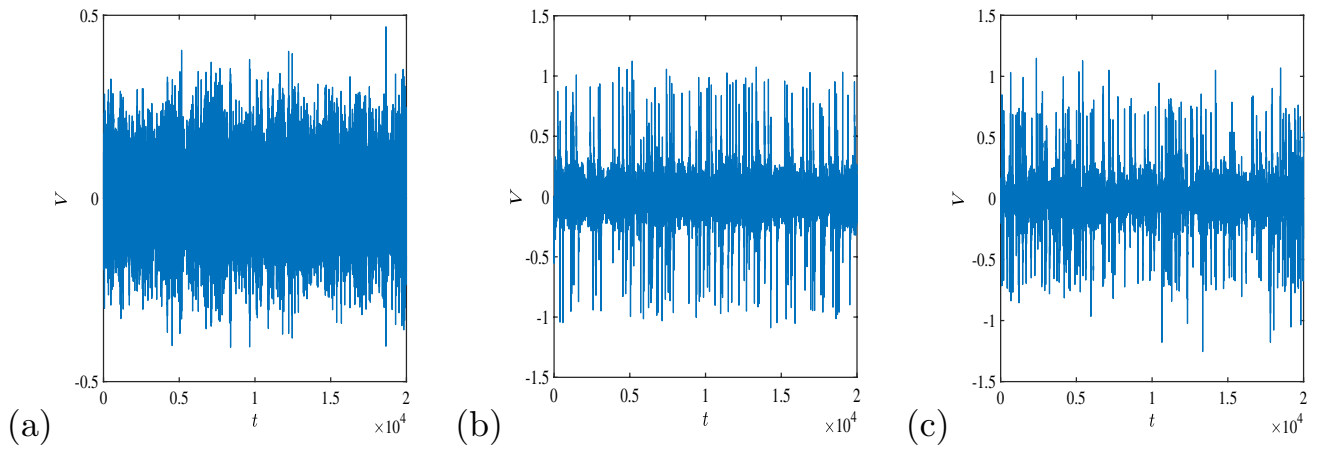

Fig. 18 Time waveform of voltage at $\sigma = 0.1$ for Fig. 16 for (**a**) nonlinear monostable, (**b**) bistable with shallow potential, (**c**) tristable

Declarations

Conflict of interest The authors declare that they have no conflict of interest.

References

1. Zhou Z, Qin W, Zhu P, Du W, Deng W, Pan J (2019) Scavenging wind energy by a dynamic-stable flutter energy harvester with rectangular wing. Appl Phys Lett 114(24):243902
2. Zhao LC, Zou HX, Gao QH, Yan G, Liu FR, Tan T, Wei KX, Zhang WM (2019) Magnetically modulated orbit for human motion energy harvesting. Appl Phys Lett 115(26):263902
3. Tao K, Yi H, Yang Y, Chang H, Wu J, Tang L, Yang Z, Wang N, Hu L, Fu Y, Miao J, Yuan W (2020) Origami-inspired electret-based triboelectric generator for biomechanical and ocean wave energy harvesting. Nano Energy 67:104197
4. Xie XD, Wang Q (2015) Energy harvesting from a vehicle suspension system. Energy 86:385–392
5. Sodano H, Inman D, Park G (2004) A review of power harvesting from vibration using piezoelectric materials. Shock Vib Dig 36:197–205
6. Erturk A, Hoffmann J, Inman DJ (2009) A piezomagnetoelastic structure for broadband vibration energy harvesting. Appl Phys Lett 94:254102
7. Litak G, Friswell MI, Adhikari S (2010) Magnetopiezoelastic energy harvesting driven by random excitation. Appl Phys Lett 96:214103
8. Kumar P, Narayanan S, Adhikari S, Friswell MI (2014) Fokker - Planck equation analysis of randomly excited nonlinear energy harvester. J Sound Vib 333:2040–2053
9. Renno JM, Daqaq MF, Inman DJ (2009) On the optimal energy harvesting from a vibration source. J Sound Vib 320:386–405
10. Adhikari S, Friswell MI, Inman DJ (2009) Piezoelectric Energy harvesting from broad band random excitations. Smart Mater Struct 18:115005
11. Xiao S, Jin Y (2017) Response analysis of the piezoelectric energy harvester under correlated white noise. Nonlinear Dyn 90:2069–2082
12. Foong MF, Thein CK, Ooi BL, Yurchenko D (2019) Increased power output of an electromagnetic vibration energy harvester through anti-phase resonance. Mech Syst Signal Proces 116:129–145
13. Zhang CL, Lai ZH, Li MQ, Yurchenko D (2020) Wind energy harvesting from a conventional turbine structure with an embedded vibro-impact dielectric elastomer generator. J Sound Vib 487:115616
14. Lu F, Lee HP, Lim SP (2003) Modeling and analysis of micro piezoelectric power generators for micro-electromechanical-systems applications. Smart Mater Struct 13:57
15. Daqaq MF (2011) Transduction of a bistable inductive generator driven by white exponentially correlated Gaussian noise. J Sound and Vib 330:2254–2664
16. Ali SF, Adhikari S, Friswell MI, Narayanan S (2011) The analysis of piezomagnetoelastic energy harvesters under broadband random excitation. J Appl Phys 109:074904
17. Fang S, Zhou S, Yurchenko D, Yang T, Liao WH (2022) Multi-stability phenomenon in signal processing, energy harvesting, composite structures, and metamaterials: A review. Mech Syst Signal Proces 166:108419
18. Liang H, Hao G, Olszewski OZ (2021) A review on vibration-based piezoelectric energy harvesting from the aspect of compliant mechanisms. Sens Actuators A 331:112743
19. Cao J, Zhou S, Wang W, Jing, (2015) Influence of potential well depth on nonlinear tristable energy harvesting. Appl Phys Lett 106 (17):173903
20. Zhang Y, Jin Y, Xu P (2020) Stochastic bifurcations in a nonlinear tri-stable energy harvester under colored noise. Nonlinear Dyn 99:879–897
21. Fu H, Yeatman EM (2019) Rotational energy harvesting using bi-stability and frequency up-conversion for low-power sensing applications: Theoretical modelling and experimental validation. Mech Syst Signal Proces 125:229–244
22. Challa VR, Prasad MG, Fisher FT (2011) Towards an autonomous self-tuning vibration energy harvesting device for wireless sensor network applications. Smart Mater Struct 20(2):025004
23. Daqaq MF (2010) Response of unimodal Duffing type harvesters to random forced excitations. J Sound Vib 329:3621–3631
24. Gao QH, Zhang WM, Zou HX, Li WB, Peng ZK, Meng G (2017) Design and Analysis of a Bistable Vibration Energy Harvester Using Diamagnetic Levitation Mechanism. IEEE Trans Magn 53(10):1–9
25. Cottone F, Gammaitoni L, Vocca H, Ferrari M, Ferrari V (2012) Piezoelectric buckled beams for random vibration energy harvesting. Smart Materials Struct 21(3):035021
26. Arrieta AF, Hagedorn P, Erturk A, Inman DJ (2010) A piezoelectric bistable plate for nonlinear broadband energy harvesting. Appl Phys Lett 297:104102
27. Sebald G, Kuwano H, Guyomar D, Benjamin D (2011) Simulation of a Duffing oscillator for broadband piezoelectric energy harvesting. Smart Materials Struct 20(7):075022
28. He Q, Daqaq MF (2014) Influence of potential function asymmetries on the performance of nonlinear energy harvesters under white noise. J Sound Vib 333(15):3479–3489
29. Jiang WA, Chen LQ (2016) Stochastic averaging based on generalized harmonic functions for energy harvesting systems. J Sound Vib 377:264–283
30. Yang T, Cao Q (2019) Dynamics and performance evaluation of a novel tristable hybrid energy harvester for ultra-low level vibration resources. Inter J Mech Sci 156:123–136
31. Yang X, Wang C, Lai SK (2020) A magnetic levitation-based tristable hybrid energy harvester for scavenging energy from low-frequency structural vibration. Eng Struct 221:110789
32. Breunung T, Balachandran B (2023) Noise color influence on escape times in nonlinear oscillators - experimental and numerical results. Theor Appl Mech Lett 13(2):100420
33. Jung P, Hänggi P (1987) Dynamical systems: A unified colored-noise approximation. Phys. Rev. A 35(10):4464–4466
34. Duan WL, Fang H (2023) The unified colored noise approximation of multidimensional stochastic dynamic system. Phys A: Statist Mech Appl 555:124624
35. Liu D, Xu Y, Li J (2017) Probabilistic response analysis of nonlinear vibration energy harvesting system driven by Gaussian colored noise. Chaos, Solitons Fractals 104:806–812
36. Risken H (1996) The Fokker-Planck Equation: Methods of Solution and Applications. Springer-Verlag, New York
37. Kumar P, Narayanan S (2006) Solution of Fokker-Planck equation by finite element and finite difference methods for nonlinear system. Sadhana 31(4):455–473
38. Kumar P, Narayanan S (2009) Numerical solution of multidimensional Fokker-Planck equation for nonlinear stochastic dynamical systems. Adv Vib Eng 8(2):153–163

39. Kloeden PE, Platen E (1992) Numerical solution of Stochastic differential Equation. Springer-Verlag, Berlin
40. Shinozuka M (1972) Monte Carlo solution of structural dynamics. Comput Struct 2(5):855–874
41. Proppe C, Pradlwarter HJ, Schuëller GI (2003) Equivalent linearization and Monte Carlo simulation in stochastic dynamics. Probab Eng Mechan 18(1):1–15